*Sensors and Materials*, Vol. 15, No. 2 (2003) 053–065
MYU Tokyo

S & M 0509

# Dependence of the Anisotropy of Wet Chemical Etching of Silicon on the Amount of Surface Coverage by OH Radicals

Miguel A. Gosálvez, Adam S. Foster and Risto M. Nieminen

Laboratory of Physics, Helsinki University of Technology,
P.O. Box 1100, 02015 Espoo, Finland

(Received September 19, 2002; accepted January 20, 2003)

***Key words:*** anisotropic etching, atomistic simulation, cellular automaton, surface coverage, convex corner, pit nucleation, step propagation

The dependence of the etch rates of different crystallographic orientations on the surface coverage by OH radicals is studied by atomistic simulations using a cellular automaton. We show that the etch rate is a non-monotonic function of OH coverage and that there always exists a coverage value at which the etch rate reaches a maximum. The dependence of the anisotropy of the etching process on coverage, including the dependence of the fastest-etched plane orientation, is implicitly contained in the model, and predictions of convex-corner under-etching structures are made. We show that the entire etching process, including the interplay between step propagation and etch pitting at any surface orientation, is controlled by only a few surface configurations involving a particular type of next-nearest neighbours.

## 1. Introduction

Anisotropic wet chemical etching of silicon in alkaline solutions[1] is one of the key techniques for the manufacture of microsystems. However, the microscopic mechanisms responsible for the strong anisotropy are still debated. It is generally thought that hydroxyl ions $OH^-$ present in the etching solution play a central role. They replace the surface-terminating hydrogens and catalyze the removal of the surface atoms by weakening their backbonds.[2] Recently, it has been shown that these substitutions are hindered at certain

surface configurations due to the interaction between the terminating hydroxyls and the terminating species (H or OH) at the next-nearest neighbours.[3] We report on the effects of the H/OH and OH/OH interactions on the etching rates of different crystallographic orientations and on the under-etched structures appearing at convex corners of masking patterns.

## 2. Microscopic Model

Anisotropic wet chemical etching is a non-equilibrium process. Thus, the initial flat/rough physical state of the surface is irrelevant for the long-time steady-state morphology reached during etching. Actually, the steady-state morphology and roughness are uniquely determined by the inherent anisotropy of the etching process. The relation between roughness/morphology and anisotropy is so strong that steady-state surface morphologies allow for the extraction of reliable, site-specific reaction rates (i.e. the anisotropy of the etching process).[4] This and other ways of roughening a surface by other means than increasing the temperature are often referred to as kinetic roughening and kinetic smoothing.[5,6] In contrast, thermal roughening is an equilibrium concept describing the spontaneous formation of disordered (rough) surfaces as a result of the dominance of the entropy contribution to the surface free energy over the surface internal energy above the roughening temperature.

These two types of roughening should not be confused. For instance, the fact that typically the surface becomes microscopically rougher as the temperature is increased during etching is due to the fact that etching is becoming more isotropic (as the slower site-specific reaction rates become comparable to the faster rates) and not to thermal roughening. In other words, kinetic roughening depends on temperature, because the anisotropy itself depends on temperature. However, this is independent of whether the equilibrium surface (with no etchant, in vacumm) is rough or flat or is changing from flat to rough in the range of temperatures considered.

The anisotropy of wet chemical etching is the result of two microscopic mechanisms:[3] the weakening of backbonds following OH termination of surface atoms, and the existence of significant interaction between these hydroxyl groups and other species (such as hydrogen and other hydroxyl groups) terminating the next-nearest neighbours. In this section we describe the two mechanisms.

### 2.1 *Backbond weakening*

Figure 1 shows the real structure and a schematic representation of one possible scenario for the removal of a surface atom (target atom A). In this particular example, the removal requires breaking the backbonds 2, 3 and 4 to the first neighbours B1-B3. The energy required to break *e.g.*, target bond 4, depends on the number of OH groups attached, not only to atom A, but also to atom B1. This is due to the fact that OH-termination of the surface atoms results in the weakening of the backbonds to the bulk. Electronic structure calculations[3] show that the weakening of any backbond depends only on the *total number* of hydroxyls attached to the two atoms sharing the bond and is independent of the particular distribution of the OH groups between the two atoms. In other words, each

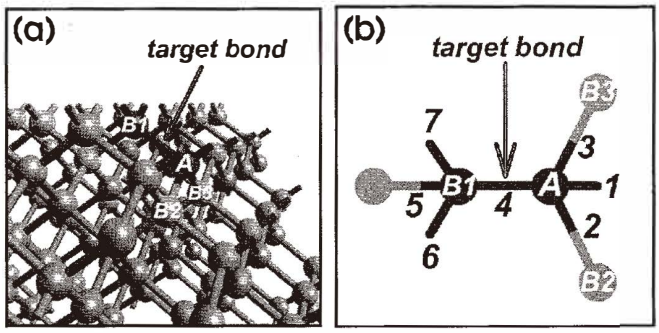


Fig. 1. A surface atom (A) in the real structure (a) and a schematic representation (b) of the inmediate neighbourhood of A, focusing on one of the three backbonds (target bond 4). OH termination of surface atoms is represented by dangling bonds.

backbond is weakened by the same energy amount ε (≈ 0.4 eV) for every OH group that is attached to either atom. In this way, the energy of a bond between an atom terminated by $i$ OH groups and an atom terminated $j$ groups ($i,j$ = 0, 1, 2, 3) can be written as

$$\varepsilon_{ij} = \varepsilon_0 - (i + j) \cdot \varepsilon , \tag{1}$$

where $\varepsilon_0$ is the bond energy between two bulk atoms ( $\varepsilon_0 \approx 2.7$ eV ).

The total bonding energy for a surface atom with $n$ first neighbours is simply the sum of the energies of the $n$ bonds:

$$E_{\text{bonds}} = \sum_{j=1}^{n} \varepsilon_{m,m_j} . \tag{2}$$

Here we have considered the most general case, in which the target atom is terminated by $m$ OH groups ($m \le 4 - n_j$) and the $j$-th first neighbour ($j$=1,2,..,$n$), having itself $n_j$ first neighbours, is terminated by $m_j$ OH groups ($m_j \le 4 - n_j$).

### 2.2 *OH/H and OH/OH interactions*

The other microscopic mechanism playing a major role in wet chemical etching, namely, the interaction between the terminating hydroxyl groups and hydrogen and/or other hydroxyl groups, occurs only in the presence of *indirect second neighbours*.[3] These are next-nearest neighbours which cannot be reached from the target atom by a covalent-bond path passing directly through a first neighbour. However, a *direct* second neighbour is linked to the target atom by a covalent path *directly* passing through a first neighbour. For instance, the second neighbours C1 through C6 in Fig. 2(a) are *direct* whilst the second neighbours C7 and C8 are *indirect*.

The presence of an indirect second neighbour imposes additional geometrical restrictions to hydroxyl termination of the target atom due to the extra interaction between the

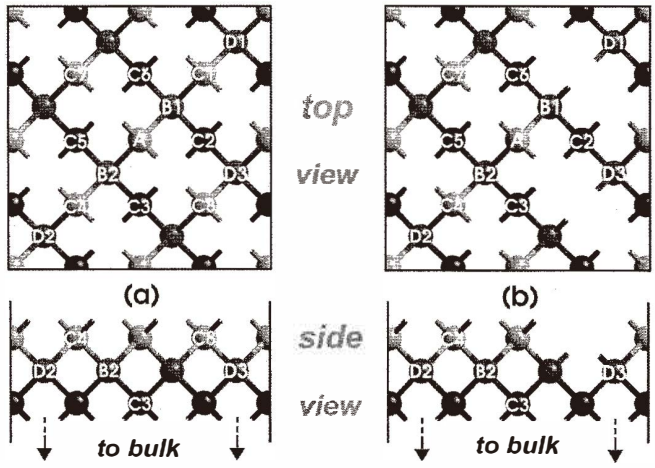


Fig. 2. (a) A typical atom (A) in an ideal (100) surface having 2 first neighbours (B12-B2) and 8 second neighbours (C1-C8). C1 through C6 are examples of *direct* second neighbours and, C7 and C8, of *indirect* second neighbours. (b) Atom A has now only 6 second neighbours (C2-C7). Note that D1 restricts the attachment of a hydroxyl onto B1 in the same manner as C7 does for A.

hydroxyl group and the terminating species (H or OH) attached to the indirect neighbour. As shown in Fig. 2(b), similar restrictions can also occur for the attachment of hydroxyl groups to the *first neighbours* of the target atom. Note that the termination state of the first neighbours has major implications for the value of the bonding energy of the target atom (Section 2.1) and, thus, the restrictions in OH-attachment at the *first neighbours* become relevant. As a result, the energy of the OH/H and OH/OH interactions can be considered to have two contributions: one from the target atom (TA) and another one from the first neighbours (FNs). Thus, the total energy of a surface atom is

$$E = E_{\text{bonds}} + \sum (e^{TA}_{OH/H} + e^{TA}_{OH/OH}) + \sum (e^{FN}_{OH/H} + e^{FN}_{OH/OH}) . \tag{3}$$

Here $E_{\text{bonds}}$ is the energy of eq. (2) and $\sum (e^{TA}_{OH/H} + e^{TA}_{OH/OH})(\sum (e^{FN}_{OH/H} + e^{FN}_{OH/OH}))$ symbolically denotes the total energy from the interactions between the OH groups terminating the target atom TA (the first neighbours FN) and H and/or OH terminating the indirect second neighbours of the target atom TA (first neighbours FN).

The geometrical restrictions to hydroxyl termination in the presence of indirect second neighbours is a manifestation of the important role of steric hindrance in anisotropic wet chemical etching. As an example of this importance, the morphological effects of isopropanol (IPA) in aqueous etchants (namely, the formation of atomistically rougher surfaces with slower macroscopic etch rates and (partial) suppression of pyramidal etch hillocks) are explained by the formation of isopropoxy-terminated sites (≡Si-OR, with $R=CH(CH_3)_2$) that are sterically hindered by the hydrocarbon chain and thus relatively

resistant to etching.[7] Our model identifies the source of steric hindrance as the (H/OH-terminated) indirect second neighbours and explicitly states that OH-terminated sites suffer from this geometrical constriction in a similar way as isopropoxy-terminated sites.

## 3. Atomistic Simulations

We carry out atomistic simulations using a continuous cellular automaton[8] developed from a discrete Monte Carlo scheme.[9] Each surface atom is characterized with a probability of removal given by the Boltzmann factor:

$$p = e^{-\Delta E / k_B T} \tag{4}$$

where the *energy excess* $\Delta E$ is defined as:

$$\Delta E = k_B T \ln\left[1 + e^{(E - E_c^A)/k_B T}\right]. \tag{5}$$

The critical energy $E_c^A$ acts as a threshold below which the removal of an atom occurs with probability p ≈ 1. The energy $E$ is given by eq. (3). Note that $\Delta E = max\ (0, E - E_c^A)$ at $T = 0$ and that, at finite temperatures, $\Delta E \approx max\ (0, E - E_c^A)$.

The effect of different OH/OH interaction energies $e_{OH/OH}^{TA}$ is considered in the simulations. For each value of $e_{OH/OH}^{TA}$, a value for $e_{OH/OH}^{FN}$ is obtained from:[10]

$$e_{OH/OH}^{FN} = e_{OH/OH}^{TA} - 0.2 \text{ eV}. \tag{6}$$

The energies $e_{OH/H}^{TA}$ and $e_{OH/H}^{FN}$ are kept fixed at 0.2 eV and 0.0 eV, respectively.[10] For the use of eq. (5), $E_c^A = 2.12$ eV and $T = 348$ K. In the simulations, hydroxyl termination of the target atom and its first neighbours (i.e., OH clustering) is assumed for all surface coverage values.[10] For the second neighbours of the target atom, one type of termination or the other (i.e. OH or H) occurs stochastically (with probability $p = \theta$ or $p = 1 - \theta$, respectively) depending on the OH-coverage value ($\theta$).

## 4. Results

We determine the effects of simultaneous surface coverage by OH and H on the etching process by considering two related problems: the dependence of the etch rates on the amount of OH coverage ($\theta$), and the under-etching structures appearing at the convex corners of masks for different values of $\theta$.

### 4.1 *Etch rates vs coverage*

In Fig. 3(a), we show the etch rates of a representative set of orientations as a function of OH coverage $\theta$. As demonstrated by the figure, the etch rate of each orientation reaches a maximum, in agreement with experiment.[11,12] This is explained as follows. As the coverage increases in the low-coverage region, the etching process becomes faster, since more OH groups provide larger amounts of weaker bonds, which are more susceptible to thermal breaking. However, as the OH coverage is further increased, the existence of OH/OH interactions between the increasing number of terminating hydroxyls eventually slows down the etching process, producing the appearence of the observed maxima. As Fig. 3(b) shows, the position of the maximum is correlated to the energy of the OH/OH interactions.

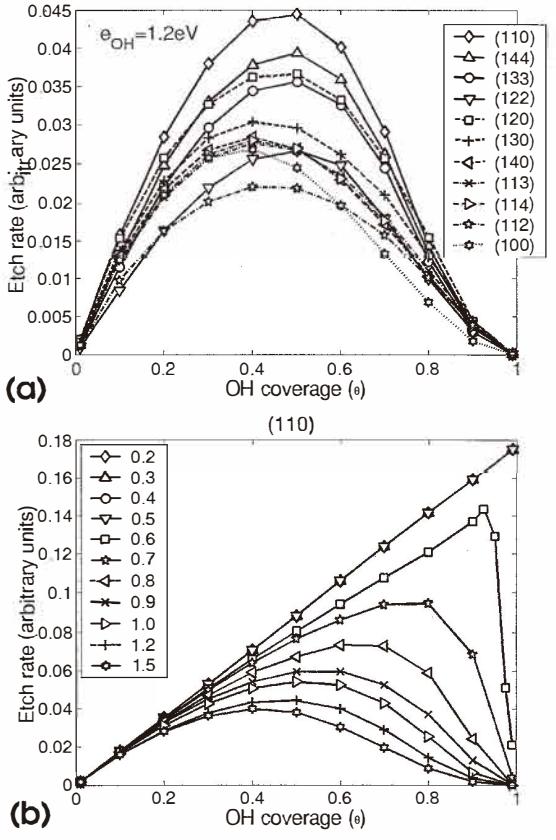


Fig. 3. (a) Etch rates of different orientations (hkl) as a function of OH coverage ($\theta$). $e^{TA}_{OH/OH}$=1.2 eV.) (b) Dependence of the etch rate of (110) on OH coverage ($\theta$) for different interaction energies $e^{TA}_{OH/OH}$ = 0.2, 0.3,..., 1.5 eV.

### 4.2 *Under-etching vs coverage*

We now consider the underetched structures that appear at the convex corners of square-shaped masks oriented at an angle $\alpha$ with the <110> direction on a Si(001)-oriented crystal. As seen from columns (a) and (b) of Fig. 4, the shape of the underetched structure depends strongly on the amount of OH coverage. In fact, the dependence is not trivial, and it is not always possible (in agreement with experiments[13]) to find the crystallographic orientation of all the appearing surface facets. As an example, the orientation of the two lower surface facets in the inset of frame (c. l) cannot be properly determined, although all the surfaces appearing in frame (b.1) can be successfully indexed. Another example is that of (311), which cannot be identified in (b.3), although it is found in (b.3) and (b.2). Note that the dramatic effects of variations in coverage on the shape of the underetched structures (as demonstrated by column (c)) are the result of the dependence of the

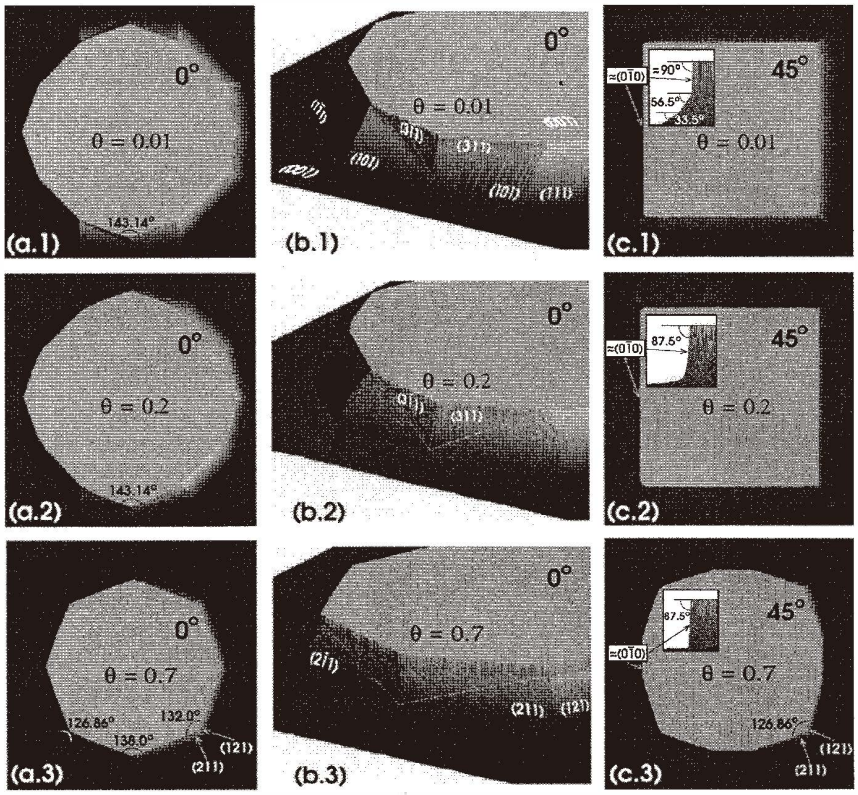


Fig. 4. Under-etching at convex corners of square-shaped masks oriented at an angle $\alpha = 0°$ (columns (a) and (b)) and $\alpha = 45°$ (column (c)) from the <110> direction on a Si(001) crystal. Three different coverage values $\theta = 0.01$ (row 1), $\theta = 0.2$ (row 2) and $\theta = 0.7$ (row 3) are shown. The planar size is $0.23 \times 0.23$ $\mu$m$^2$ and the etched depth is 18 nm in all cases. $e^{TA}_{OH/OH} = 0.6$ eV.

orientation of the fastest-etched plane on coverage. At low coverage, the etch rate of high-index planes such as (211) is not large enough as to compete with that of the (100) planes ((c.1) and (c.2)). However, at higher coverage, the etch rate of the (211) planes becomes faster and, as a result, they appear as the conforming facets at the convex corners (c.3).

The dependence of the fastest-etched plane on the amount of OH coverage is best observed with the use of a wagon-wheel masking pattern.[14] Figure 5 presents simulations of the etching of Si(001) wafers masked using that pattern for different coverage values $\theta = 0.01$, $\theta = 0.5$, $\theta = 0.7$, and $\theta = 0.9$. The figure shows that the larger the coverage, the stronger the anisotropy of the pattern. This is due to the fact that, as the amount of OH coverage increases, the etch rate of (100) planes decreases while the etch rates of other planes is still increasing. This allows other high-index planes to become the fastest-etched planes.

The microscopic model describes also the *time evolution* of the surface morphology. As an example, the typical time evolution of the undercutting process occurring at the convex corners in Fig. 4(c.3) is presented at the right-hand-side column of Fig. 6. In addition, the

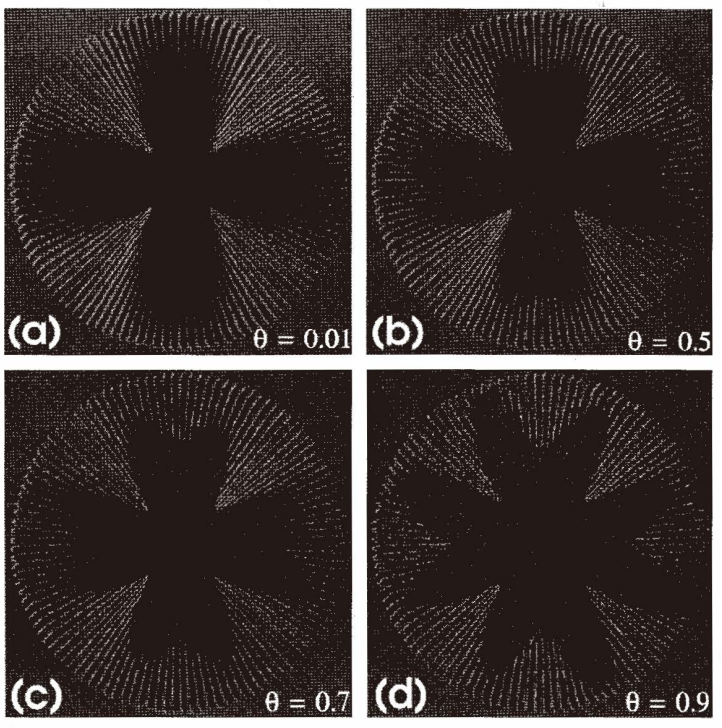


Fig. 5. Etching of Si(001) wafers masked with a wagon wheel pattern for different OH coverage values: (a) $\theta = 0.01$, (b) $\theta = 0.5$, (c) $\theta = 0.7$, and (d) $\theta = 0.9$. The planar size of the systems is $0.35 \times 0.35\ \mu m^2$.

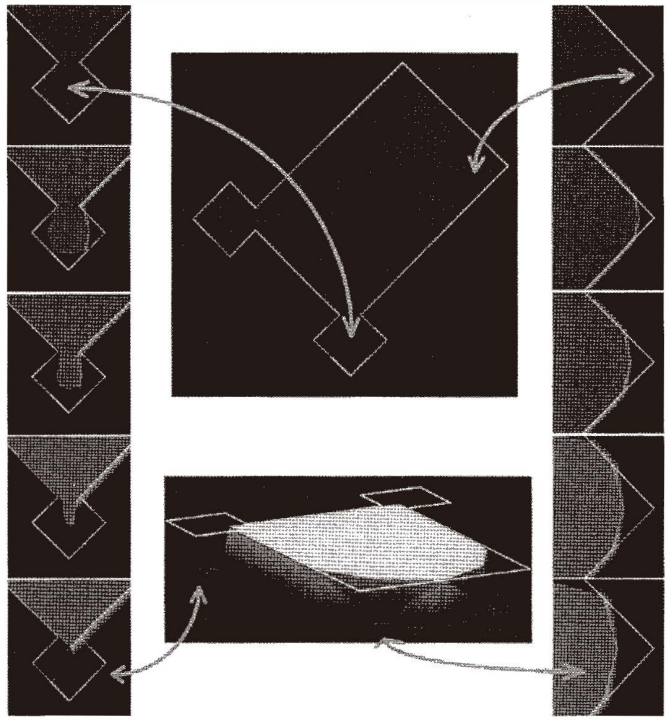

Fig. 6. Time evolution for the convex corners shown in Fig. 4(a.1) (right column) and for a typical convex-corner compensating structure[15] $\theta = 0.7$ (left column). Planar size: $0.23 \times 0.23$ $\mu$m$^2$.

time evolution for a typical convex-corner compensating structure[15] is shown on the left-hand-side column of the figure. As in the experiments, the compensating structure provides the elimination of undercutting. The microscopic model predicts that after a certain time/depth, the corner will present a desired 90 degree form (as seen from the top).

## 5. Discussion

The relative occurrence of etch pitting and step propagation in wet chemical etching is controlled by the relative values of the removal probabilities of a few surface configurations. As an example, if $(n_1,n_2)$ refers to a surface atom with $n_1$ first neighbours and $n_2$ second neighbours, and $p(n_1,n_2)$ to its removal probability, the etching process at (111) surfaces is controlled by:

$p(3,9) \leftrightarrow$ generation of pits (atom A in Fig. 7(b)),

$p(3,7) \leftrightarrow$ propagation of $[1\bar{2}1]$ steps (atom A in Fig. 7(c)),

$p(2,7) \leftrightarrow$ propagation of $[\bar{1}2\bar{1}]$ steps (atom A in Fig. 7(d)).

The microscopic processes determining the values of p(3,9), p(3,7) and p(2,7) are different in nature. Both (3,9) and (3,7) atoms have no indirect second neighbours (Fig. 7(b) and 7(c)). Thus, no dependence on the OH/OH interactions exists and the values of p(3,9) and p(3,7) are determined by the bond-weakening mechanism only. p(3,9) is typically small (negligible) as compared to p(3,7), because two of the first neighbours of A (Fig. 7(c)) are in the etch front and OH groups can be attached to them, resulting in further weakening of the backbonds of A. In the case of atom A in Fig. 7(d), the appearence of one indirect second neighbour (i) reduces the probability of OH termination of the dangling bond DB2 with respect to that of DB1, especially at higher coverages, where the interaction between terminating OHs is more frequent. Therefore, there is a reduction in the rate of $[\bar{1}2\bar{1}]$-step propagation with increasing coverage. Since the faster $[1\bar{2}1]$-steps will eventually disappear in favour of the slower, more stable $[\bar{1}2\bar{1}]$-steps, the etching of the (111) surfaces at higher coverages can be thought to occur by $[\bar{1}2\bar{1}]$-step propagation only. At low coverage, the situation will be the reverse. Thus, triangular pits on the (111) surface should be bounded by $[\bar{1}2\bar{1}]$-steps for conditions providing large coverage by hydroxyl groups,

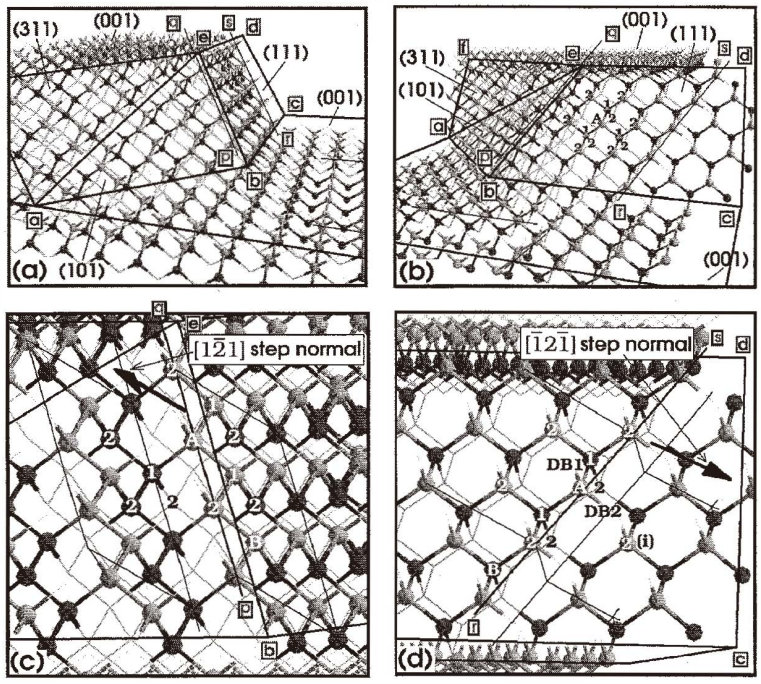


Fig. 7. (a) An underetched convex corner at low $\theta$ (*cf.* Fig. 4(b.1)). (b) A different view of (a). Closer views of (c) a $[1\bar{2}1]$ step and (d) a $[\bar{1}2\bar{1}]$ step are shown from arbitrary directions.

and by $[1\bar{2}1]$-steps for low coverage. Moreover, hexagonal pits should arise at intermediate values of coverage within some coverage range R. The location of R along the coverage-axis (e.g. towards higher or lower coverages) should be correlated to the energies of the OH/H and OH/OH interactions, as particular values for these interactions can be considered to characterize the surface substitutions of hydrogen by hydroxyl for each particular etchant. The energies being different, the concentrations of different etchants providing the same coverage will also be different.

The previous considerations explain the experimental fact that, for 25 wt.% TMAH aqueous solution at 80°C, the triangular pits have edges with two-backbonded atoms (i.e., $[1\bar{2}1]$-steps)[16] whilst hexagonal pits exhibiting the two types of steps simultaneously are found at a smaller concentration of 20 wt.% at the same temperature.[17] According to the experimental contour plots of the etch rate derived from hemispherical specimens at other temperatures (70°C and 90°C) in the same etchant,[18] hexagonal pits should be expected at lower concentrations (20 wt.%) and $[1\bar{2}1]$-edged triangular pits for higher concentrations (25 wt.%). No experimental data concerning concentrations below 20 wt.% TMAH (for which $[1\bar{2}1]$-edged triangular pits would be present) was found by the authors.

For KOH as the etchant, the fact that the triangular pits are made of steps with three-backbonded atoms (i.e., $[1\bar{2}1]$-steps) for 17, 26, 34 and 40 wt.%[16] implies that rather high concentrations are required for this etchant to provide substantial OH-coverage of the surface. This is attributed to large OH/H and OH/OH interactions for the replacement of surface terminating hydrogens. No experimental data concerning higher KOH concentrations (for which $[\bar{1}2\bar{1}]$-edged triangular pits would be present) was found by the authors.

The formation of monohydride-terminated and vertical dihydride-terminated triangular pits (with $[1\bar{2}1]$-steps and $[\bar{1}2\bar{1}]$-steps, respectively) as well as hexagonal pits, as a function of the relative reaction rates of the monohydride and dihydride surface sites, has been shown by Flidr *et al.* by means of Monte Carlo simulations.[4] We note, however, that the dependence of the shape of the pits (i.e., triangular up, hexagonal or triangular down) on concentration cannot be understood from their approach, as they can change the reaction rates of the different sites at will but cannot elaborate on the reason why the values of these reaction rates would change with concentration. Our model, however, describes how this change occurs with coverage.

Similar analysis of other orientations shows that the etching process is always controlled by a reduced number of surface configurations. For instance, the etch rate of (100) surfaces is controlled by

p(2,8) $\leftrightarrow$ generation of etch pits,

p(2,7) $\leftrightarrow$ propagation of [110] and $[1\bar{1}0]$-steps.

As in the case of p(2,7), p(2,8) depends strongly on the OH/OH interactions and becomes very small at large coverages. Other examples are the (110) surfaces, controlled by p(3,7); the (311) surfaces, controlled by p(3,7) and p(2,7); or the (211) surfaces, controlled by p(3,9) and p(2,7).

The previous analysis shows that the dependence of the orientation of the fastest-etched planes on coverage can be understood as the macroscopic manifestation of the geometrical

restrictions imposed by the indirect second neighbours. Through these geometrical restrictions, the amount of OH coverage $\theta$ fixes the relative value of the removal probabilities p(2,7) and p(2,8) with respect to p(3,7) and p(3,9), i.e. the relative occurrence of step propagation and etch pitting at all orientations.

Hines *et al.* have attempted to explain qualitatively the anisotropy of the etching process by means of bond strain and structural rigidity considerations associated to the formation of a (postulated) pentavalent transition state.[19] The geometry of this pentavalent transient presumably involves significant distortion of the tetrahedral geometry (tetravalent state). Thus, the argument is to compare how close the geometry of the surface site is to the (unknown) geometry of the transient and to determine the amount of rigidity around the site in order to correlate (qualitatively) these two aspects to the reactivity of the site. This is possible because, in principle, strained surface sites have already a distorted tetrahedral geometry and, thus, should present lower activation energies to the pentavalent transition state and, as a result, large reaction rates. One should notice, however, the fact that some 'strained sites' (such as e.g. the vertical dihydride) preserve near tetrahedral geometry in the strained state,[19] and therefore, are not any closer to the transition state than unstrained sites. Thus, the correlation between strain and reactivity should be done taking special care that only internal strains of the tetrahedral geometry are considered, not strained states of the entire tetrahedron with respect to the surface. Additionally, structural rigidity around the site should be considered as it can dramatically suppress reactivity by preventing the required distortion into the pentavalent transition state.[19] The structural rigidity of a surface site is a property of the neighbourhood, not of the site itself: it concerns the rigidity of the bonds of the first neighbours to the rest of the structure, not the rigidity of the bonds of the site itself.

Interestingly, Hines *et al.* have systematically tried to correlate reactivity to strain only,[4,7,20,21] disregarding the essential role of structural rigidity. We venture that the reason for this lies probably in the fact that, at first glance, the internal strain of the tetrahedral state and the structural rigidity of the site are (inversely) correlated: if a site displays large distortion of the tetrahedral geometry, the distortion must be enabled by low structural rigidity. Therefore, it would seem that the use of only one of the two measures (*e.g.*, strain) should be sufficient for characterization of the site reactivity. This is, however, not the case. Unstrained states are possible without (significant) structural rigidity: the unstrained point site (an isolated horizontal dihydride) is an example of such case.[20] Therefore, the use of internal strain of the tetrahedral geometry as an indicator of reactivity is not suitable. The situation is not eased by the use of strained states of the entire tetrahedron (not internal strains), as in the case of the vertical dihydride.[19] In our opinion, the structural rigidity of the site represents a more accurate measure of reactivity. In a way, this is precisely what our model does. By taking into account steric hindrance for both the target atom and the first neighbours, an account of structural rigidity is provided. This explains the fact that oxidation in aqueous solutions (i.e., substitution of H by OH) cannot be correlated to local strain.[21] The fact that the unstrained point site is approximately 1 order of magnitude more reactive than the highly strained vertical dihydride step site, as stated in ref. (21), can be explained in the framework of our model: the vertical dihydride, having one indirect second neighbour, suffers from steric hindrance whilst the point site does not.

## 6. Conclusions

It has been shown that, for every crystallographic orientation, there always exists a value of coverage for which the etch rate reaches a maximum, in agreement with experiments.[11,12] The dependence of the fastest-etched plane orientation on coverage is controlled by only a few surface configurations whose removal probabilities determine the relative occurrence of step propagation and etch pitting for all orientations. The microscopic model explains the dependence of the anisotropy of the etching process on coverage, including the dependence of the fastest-etched plane orientation, and allows for predictions of convex-corner under-etching structures. It has been shown that the use of local strain as an indicator of site reactivity is not suitable. Instead, the structural rigidity of the site (*e.g.*, as accounted for by our model) represents a more accurate measure of reactivity.

### References


1 W. Lang: Materials Science and Engineering R: Reports: A Review Journal **17** (1996) 1.
2 P. Allongue: Phys. Rev. Lett. **77** (1996) 1986.
3 M. A. Gosálvez, A. S. Foster and R. M. Nieminen: Europhys. Lett. **60** (2002) 467.
4 J. Flidr, Y-C. Huang and M. A. Hines: J. Chem. Phys. **108** (1998) 5542.
5 E. van Veenendaal, P. van Beurden, J. van Suchtelen and W. J. P. van Enckevort: J. Appl. Phys. **88** (2000) 4595.
6 J. H. Schmid, A. Ballestad, B. J. Ruck, M. Adamcyk and T. Tiedje: Phys. Rev. B **65** (2002) 1553115.
7 T. A. Newton, Y-C. Huang, L. A. Lepak and M. A. Hines: J. Chem. Phys. **111** (1999) 9125.
8 Zhenjun Zhu and Chang Liu: Computer Modelling in Engineering and Sciences **1** (2000) 11.
9 M. A. Gosálvez, R. M. Nieminen, P. Kilpinen, E. Haimi and V. Lindroos: Appl. Surf. Sci. **178** (2001) 7.
10 M. A. Gosálvez, A. S. Foster and R. M. Nieminen: Appl. Surf. Sci. **202** (2002) 160.
11 M. Shikida, K. Sato, K. Tokoro and D. Uchikawa: Sensors and Actuators A **80** (2000) 179.
12 I. Zubel: Sensors and Actuators A **70** (1998) 260.
13 H. Schröder and E. Obermeier: J. Micromech. Microeng. **10** (2000) 163.
14 H. Seidel, L. Csepregi, A. Heuberger and H. Baumgartel: J. Electrochem. Soc. **137** (1990) 3612.
15 B. Puers and W. Sansen: Sensors and Actuators A **21-23** (1990) 1036.
16 K. Sato, T. Masuda and M. Shikida: Proceedings of the 3rd Workshop on Physical Chemistry of Wet Chemical Etching of Silicon, June 4–6, 2002, Nara, Japan.
17 E. van Veenendaal, K. Sato, M. Shikida and J. van Suchtelen: Sensors and Actuators A **93** (2001) 219.
18 K. Sato, M. Shikida, T. Yamashiro, K. Asaumi, Y. Iriye and M. Yamamoto: Sensors and Actuators A **73** (1999) 131.
19 M. A. Hines, Y. J. Chabal, T. D. Harris and A. L. Harris: J. Chem. Phys. **101** (1994) 8055.
20 J. Flidr, Y-C. Huang, T. A. Newton and M. A. Hines: Chem. Phys. Lett. **302** (1999) 85.
21 S. P. Garcia, H. Bao, M. Manimaran, and M. A. Hines: J. Phys. Chem. B **106** (2002) 8258.